

Provided for non-commercial research and education use.
Not for reproduction, distribution or commercial use.



This article appeared in a journal published by Elsevier. The attached copy is furnished to the author for internal non-commercial research and education use, including for instruction at the authors institution and sharing with colleagues.

Other uses, including reproduction and distribution, or selling or licensing copies, or posting to personal, institutional or third party websites are prohibited.

In most cases authors are permitted to post their version of the article (e.g. in Word or Tex form) to their personal website or institutional repository. Authors requiring further information regarding Elsevier's archiving and manuscript policies are encouraged to visit:

<http://www.elsevier.com/copyright>



Contents lists available at ScienceDirect

Journal of Luminescence

journal homepage: www.elsevier.com/locate/jlumin

Optical spectroscopy of lanthanides doped in wide band-gap semiconductor nanocrystals

Yongsheng Liu^{a,b}, Wenqin Luo^{a,b}, Haomiao Zhu^{a,b}, Xueyuan Chen^{a,b,*}^a Key Laboratory of Optoelectronic Materials Chemistry and Physics, Fujian Institute of Research on the Structure of Matter, Chinese Academy of Sciences, Fuzhou, Fujian 350002, China^b State Key Laboratory of Structural Chemistry, Fuzhou, Fujian 350002, China

ARTICLE INFO

Available online 30 July 2010

Keywords:Lanthanides
Semiconductor nanocrystals
Electronic structure
Excited-state dynamics
Photoluminescence

ABSTRACT

Currently, tripositive lanthanide (Ln^{3+}) ions doped wide band-gap semiconductor nanocrystals (NCs) have been the focus of research interest due to their distinct optical properties and potential applications in optical devices and luminescent biolabels. Because of the low absorptions of parity-forbidden 4f–4f transitions for Ln^{3+} , it is highly anticipated that the luminescence of Ln^{3+} ions embedded in wide band-gap NC lattices can be sensitized efficiently via exciton recombination in the host. For this purpose, the successful incorporation of Ln^{3+} into the lattices of semiconductor NCs is of utmost importance, which still remains intractable via conventional wet chemical methods. Here, the most recent progress in the optical spectroscopy of Ln^{3+} ions doped wide band-gap semiconductor NCs is discussed. Much attention was focused on the optical properties including electronic structures, luminescence dynamics, energy transfer as well as the up-conversion emissions of Ln^{3+} ions in ZnO , TiO_2 , SnO_2 and In_2O_3 NCs that were synthesized in our laboratory using wet chemical methods.

© 2010 Elsevier B.V. All rights reserved.

1. Introduction

Tripositive lanthanide (Ln^{3+}) ions doped inorganic nanocrystals (NCs) with various compositions have become an increasing research topic and opened up the opportunity for creating new applications in diverse fields such as light emitting displays, biological labeling and imaging, owing to their distinct electrical and optical properties [1–3]. Because of the large surface to volume ratio as well as the quantum confinement effect, physicochemical properties of the host materials in nanoscale may differ markedly from those in the bulk, affecting the luminescence properties and excited-state dynamics of the doped Ln^{3+} ions [4]. In particular, it is highly desired that luminescence of Ln^{3+} ions embedded in wide band-gap semiconductor NCs can be efficiently sensitized by exciton recombination in the host, since direct excitation of the parity forbidden 4f–4f transitions of Ln^{3+} is generally inefficient compared to the host absorption in ultraviolet (UV) region. For this purpose, considerable efforts have been devoted to the synthesis and tuning of optical properties of Ln^{3+} ions doped in semiconductor NCs. To date, efficient emissions of Ln^{3+} have been achieved via host sensitization. However, it should be noted that, in most cases, only broad emission lines could be observed due to poor

incorporation of Ln^{3+} ions into the lattices of semiconductor NCs [5–8]. We expect that the incorporation of various Ln^{3+} ions in the lattices of semiconductor NCs can lead to sharp and multicolor emissions from Ln^{3+} to meet the increasing demands for highly sensitive biolabeling, lighting and displays. Very recently, utilizing facile sol–gel and solvothermal methods, we have successfully incorporated Ln^{3+} ions in the lattices of different semiconductor NCs such as ZnO , SnO_2 , TiO_2 and In_2O_3 [9–15]. As a result, intense and sharp emission lines of Ln^{3+} ions have been realized in most semiconductor NCs via host sensitization. The optical properties of Ln^{3+} in semiconductor NCs, including electronic structures, energy transfer (ET), excited-state dynamics as well as up-conversion (UC) luminescence, have been investigated in detail.

This work focuses primarily on the photoluminescence (PL) properties of Ln^{3+} ions doped in wide band-gap semiconductor NCs that were synthesized using wet chemical methods. We first demonstrate the electronic structures and then the excited-state dynamics of Ln^{3+} ions embedded in semiconductor NCs. In Section 4, we highlight the host sensitized luminescence of Ln^{3+} ions. Finally, the UC luminescence originating from Ln^{3+} ions doped in TiO_2 NCs is also discussed in Section 5.

2. Electronic structures of Ln^{3+} ions

The electronic structures of Ln^{3+} ions are critically dependent on the local symmetry around Ln^{3+} ions [4]. A small difference in

* Corresponding author at: Key Laboratory of Optoelectronic Materials Chemistry and Physics, Fujian Institute of Research on the Structure of Matter, Chinese Academy of Sciences, Fuzhou, Fujian 350002, China. Tel./fax: +86 591 8764 2575.
E-mail address: xchen@fjirsm.ac.cn (X. Chen).

local structure will lead to significant change in the electronic energy levels as well as excited-state dynamics of the doped Ln^{3+} ions. In nanoscale, structure disordering and surface defects are inevitable after the introduction of Ln^{3+} ions into the lattices of wide band-gap semiconductor NCs. Consequently, multiple sites of Ln^{3+} with different crystal-field (CF) surroundings will come into being [11,16–18]. In view of the diverse CF surroundings, Ln^{3+} ions occupying multiple sites in semiconductor NCs are expected to exhibit distinct PL and luminescence decays for each single site. These optical features thereby facilitate the probe into the local structures of Ln^{3+} ions in semiconductor NCs using the site-selective and time-resolved spectra.

2.1. $\text{TiO}_2:\text{Eu}^{3+}$ NCs

Recently, we have provided solid evidence of multiple sites of Eu^{3+} in anatase TiO_2 aggregates assembled from 10–12 nm TiO_2 NCs [11]. By means of site-selective spectroscopy at 10 K, three types of luminescence centers of Eu^{3+} (marked as sites I–III) in TiO_2 NCs were identified. As compared in Fig. 1, the PL excitation and emission patterns differed obviously from each other in line positions, shapes and intensities, indicative of a totally different CF environment experienced by Eu^{3+} ions in $\text{TiO}_2:\text{Eu}^{3+}$ NCs. One site (site I) exhibited broadened fluorescence lines with the most

intense emission at 613.3 nm similar to that of Eu^{3+} in glasslike phase, which was related to the distorted lattice site near the surface. The other two sites (sites II and III) presented sharp emission and excitation lines with the most intense peaks at 616.7 and 618.1 nm, respectively, which originated from lattice sites with ordered crystalline environment in anatase TiO_2 . Similar multiple sites of Eu^{3+} were also detected in $\text{ZnO}:\text{Eu}^{3+}$ NCs synthesized using the modified sol-gel method [16].

It is well known that the luminescence of Eu^{3+} is usually utilized as a sensitive structural probe to investigate the coordination and local environment around cations, considering the fact that the $^5\text{D}_0$ (or $^7\text{F}_0$) level is nondegenerate and splitting of the emission transitions reflects the CF splittings of the normal $^7\text{F}_j$ levels [19]. By carefully analyzing the high resolution emission and excitation spectra of Eu^{3+} ions in TiO_2 NCs at 10 K (Fig. 1), the local symmetries of two lattice sites could be determined based on the J–O theory, the selection rules for electric-dipole (ED) and magnetic-dipole (MD) transitions of Eu^{3+} ions [20,21]. In anatase TiO_2 structure, Ti^{4+} ions sit at a D_{2d} lattice site. The substitution of Ti^{4+} with the larger Eu^{3+} will lead to the descent of intrinsic D_{2d} to a lower site symmetry (S_4 , C_{2v} or D_2), according to branching rules of the 32 point groups [22]. If Eu^{3+} ions were situated at the D_{2d} or S_4 lattice sites, only two lines for the $J=0$ to $J=1$ transition and three lines (S_4) or two lines (D_{2d}) for the $J=0$ – $J=2$ CF transition should be detected. Nevertheless, three lines for the $^5\text{D}_0 \rightarrow ^7\text{F}_1$ transition and four lines for the $^5\text{D}_0 \rightarrow ^7\text{F}_2$ transition of Eu^{3+} ions at site II can be clearly identified. Moreover, according to the ED selection rule, the $^5\text{D}_0 \rightarrow ^7\text{F}_0$ (0–0) transition is allowed only in the following 10 site symmetries, C_s , C_1 , C_n , and C_{nv} ($n=2, 3, 4, 6$) [19,23]. The appearance of the 0–0 line suggests that Eu^{3+} ions at site II may occupy a highest symmetry of C_{2v} . In contrast, for Eu^{3+} at site III, the absence of 0–0 emission and three resolved lines from the emission of $^5\text{D}_0 \rightarrow ^7\text{F}_1$ plus three lines from the emission of $^5\text{D}_0 \rightarrow ^7\text{F}_2$ indicates a possible D_2 site symmetry for site III. As for Eu^{3+} at site I, it resides in a disordered environment and therefore possesses the lowest site symmetry C_1 .

2.2. $\text{TiO}_2:\text{Er}^{3+}$ NCs

Interestingly, by slightly modifying the synthesis condition (reaction temperature), only one single lattice site emission of Er^{3+} in TiO_2 NCs was obtained in spite of the large mismatch of ionic radius and charge imbalance between Er^{3+} and Ti^{4+} [14], which was very different from that observed in Eu^{3+} ions doped TiO_2 NCs. Fig. 2a showed the 10 K excitation spectrum of Er^{3+} doped TiO_2 NCs when monitoring the near-infrared (NIR) $^4\text{I}_{13/2} \rightarrow ^4\text{I}_{15/2}$ emission at 1532.6 nm. Abundant sharp excitation

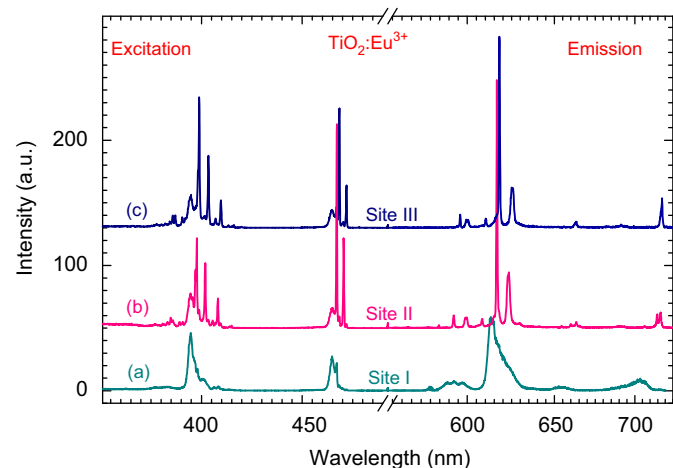


Fig. 1. The 10 K excitation spectra of $\text{TiO}_2:\text{Eu}^{3+}$ NCs (left) annealed at 400 °C by monitoring the $^5\text{D}_0 \rightarrow ^7\text{F}_2$ emissions at (a) 613.3 nm, (b) 616.7 nm and (c) 618.1 nm for sites I–III, respectively, and the 10 K emission spectra of $\text{TiO}_2:\text{Eu}^{3+}$ (right) annealed at 400 °C, with (a) $\lambda_{\text{exc}}=464.6$ nm for site I, (b) $\lambda_{\text{exc}}=470.7$ nm for site II and (c) $\lambda_{\text{exc}}=472.1$ nm for site III.

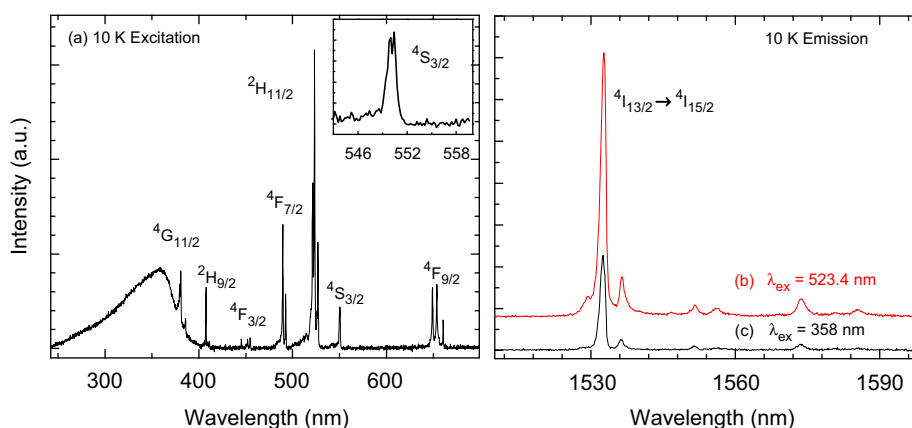


Fig. 2. The 10 K excitation spectrum (a) of $\text{TiO}_2:\text{Er}^{3+}$ NCs (the inset enlarged the excitation lines for the transition of $^4\text{I}_{15/2} \rightarrow ^4\text{S}_{3/2}$) and the 10 K NIR luminescence spectra for $\text{TiO}_2:\text{Er}^{3+}$ NCs when (b) directly and (c) indirectly excited at 523.4 and 358 nm, respectively.

lines of Er^{3+} centered at 380.6, 407.6, 489.4, 523.4, 550.5 and 654.0 nm were observed, which corresponded to the direct excitation from ground state of $^4\text{I}_{15/2}$ to the upper excited states of $^4\text{G}_{11/2}$, $^2\text{H}_{9/2}$, $^4\text{F}_{7/2}$, $^2\text{H}_{11/2}$, $^4\text{S}_{3/2}$ and $^4\text{F}_{9/2}$, respectively. Fine CF splitting of the excited states of Er^{3+} was distinguishable, suggesting that Er^{3+} ions were located at a lattice site rather than on the surface of TiO_2 NCs. According to the Kramers degeneracy of f^{11} configuration for Er^{3+} , two excitation lines from the lowest CF level of $^4\text{I}_{15/2}$ – $^4\text{S}_{3/2}$ were theoretically expected for Er^{3+} ions at a lattice site at 10 K. As clearly presented in the inset of Fig. 2a, there were only two lines assigned to the excited state of $^4\text{S}_{3/2}$ and no trace of CF splitting due to another site could be detected, which is in good agreement with the theoretical prediction, verifying the homogeneous CF environment (i.e. the single lattice site) for the doped Er^{3+} ions. The homogeneous CF environment for Er^{3+} in TiO_2 NCs was further confirmed by the similar NIR emission lines under different excitation paths (Fig. 2b and c). From the viewpoint of spectroscopy, we speculated that most of Er^{3+} ions were very likely located at the substitutional Ti^{4+} lattice site with a site symmetry descending from D_{2d} to C_{2v} , as revealed in Eu^{3+} doped TiO_2 NCs [11].

On the basis of the high resolution emission and excitation spectra at 10–300 K, 45 CF levels of Er^{3+} in TiO_2 NCs could be located and assigned in Table 1, which spanned the energy region of 0–27 000 cm^{-1} and belonged to 12 different SLJ multiplets of the $4f^{11}$ electronic configuration of Er^{3+} . Subsequently, energy-level fitting was performed by means of parametrization of an effective operator Hamiltonian using the f-shell empirical programs from Reid [24]. The CF analysis for Er^{3+} in anatase TiO_2 NCs at C_{2v} symmetry yielded a smaller final root-mean-square deviation of 25.1 cm^{-1} compared to that at D_{2d} symmetry (31.7 cm^{-1}), and thus verified the rationality of the C_{2v} symmetry assignment of Er^{3+} in TiO_2 NCs.

2.3. $\text{ZnO}:\text{Nd}^{3+}$ NCs

In addition to the site-selective spectroscopy, time-resolved PL (TRPL) technique is also a useful means to identify multiple Ln^{3+} sites in semiconductor NCs. Because of the very close CF levels ($\sim 13 \text{ cm}^{-1}$) of $^4\text{F}_{3/2}$ for various Nd^{3+} ions in ZnO NCs, we were unable to select PL from single Nd^{3+} site by the site-selective spectroscopy aforementioned [9]. In sharp contrast, such multiple Nd^{3+} sites in ZnO NCs could be readily distinguished from each other despite the low resolution (10 nm) of the TRPL spectra. Fig. 3 shows the TRPL spectra of $\text{ZnO}:\text{Nd}^{3+}$ NCs collected at different delay time ranging from 0 to 85 μs . It was found that the intensity of emission peak centered at 1066 nm (peak A) increased dramatically with increase in delay times, reaching the maximum at $\sim 10 \mu\text{s}$, and then became undetectable after a delay time of $\sim 30 \mu\text{s}$. Nevertheless, a much slower time evolution process was observed for emission peak at 1082 nm (peak B). The noticeable difference in the evolution of peaks A and B was mainly caused by the multiple luminescence centers of Nd^{3+} ions in the lattice sites of ZnO NCs, which possessed various CF surroundings and thus different decay behaviors [9]. Our results demonstrated here in $\text{ZnO}:\text{Nd}^{3+}$ NCs suggest that the TRPL technique can be extended to other Ln^{3+} ion doped nanomaterials with different luminescence centers, offering a remarkably higher detection sensitivity compared to the steady-state PL detection.

3. Excited-state dynamics of lanthanides

3.1. Luminescence lifetime

Luminescence lifetime (τ) is determined by radiative and nonradiative decay rates, which is closely related to the

Table 1
Energy levels of Er^{3+} at the C_{2v} site in TiO_2 NCs at 10 K.

Multiplet	Energy (cm^{-1})		ΔE (cm^{-1}) ^a	
	Exp. fit	Fit		
$^4\text{I}_{15/2}$	0	–19	–19	
	15	7	–8	
	95	81	–14	
	166	166	0	
	210	219	9	
	378	392	14	
	454	469	15	
	504	506	2	
	$^4\text{I}_{13/2}$	6525	6525	0
		6533	6543	–10
6585		6594	9	
6649				
6745				
$^4\text{I}_{11/2}$		6851		
		6859		
		10,166		
		10,184		
	10,205	10,206	1	
$^4\text{I}_{9/2}$		10,268		
		10,328		
		10,330		
		12,252		
		12,287		
		12,401		
		12,453		
	12,588	12,584	–4	
	$^4\text{F}_{9/2}$	15,140	15,122	
		15,242	15,263	–7
15,291		15,303	21	
15,404		15,383	12	
18,165		18,152	–13	
$^4\text{S}_{3/2}$	18,183	18,195	–12	
	18,975	18,972	–3	
	19,010	19,025	15	
	19,104	19,086	–18	
	19,148	19,152	4	
$^2\text{H}_{11/2}$	19,181	19,201	20	
	19,226	19,215	–11	
	20,298	20,320	22	
	20,392	20,400	8	
	20,430	20,418	–12	
	20,466	20,453	–13	
	21,997	22,049	52	
	22,119	22,117	–2	
	22,217	22,161	–56	
	$^4\text{F}_{7/2}$	22,386	22,381	–5
22,444		22,452	8	
24,298		24,283	–15	
24,313		24,295	–18	
24,411		24,406	–5	
$^4\text{F}_{5/2}$	24,426	24,442	16	
	24,525	24,546	21	
	25,920	25,991	71	
	26,062	26,031	–31	
	26,170	26,160	–10	
$^4\text{F}_{3/2}$	26,264	26,244	–20	
	26,344	26,359	15	
	26,427	26,397	–30	
	$^2\text{H}_{9/2}$			
$^4\text{G}_{11/2}$				

^a Energy difference $\Delta E = E_{\text{fit}} - E_{\text{exp}}$.

crystalline environment around the dopants [4]. Since there exist multiple luminescence centers of Ln^{3+} ions that possess various CF surroundings as discussed in Section 2, different luminescence decay curves of Ln^{3+} ions can be anticipated in Ln^{3+} ions doped semiconductor NCs. For example, by monitoring the site-selective emission ($^5\text{D}_0 \rightarrow ^7\text{F}_2$) at 10 K, two types of luminescence decays of Eu^{3+} were obtained in $\text{ZnO}:\text{Eu}^{3+}$ NCs (Fig. 4a) [12]. For Eu^{3+} at surface site (site A), the decay curve exhibited a single

exponential behavior, and the 5D_0 lifetime was determined to be 0.75 ms. Unlike Eu^{3+} ions at site A, the decay curve from 5D_0 of Eu^{3+} at lattice site (site B) showed a noticeable rising edge at the initial stage and a single exponential decay in the tail when excited to the 5D_2 state. The intrinsic lifetime of 5D_0 was determined to be 1.25 ms from the tail at 10 K.

Similar single exponential decay was also detected in Er^{3+} ions doped TiO_2 NCs. As shown in Fig. 4b, the decay curve of $^4S_{3/2}$ of

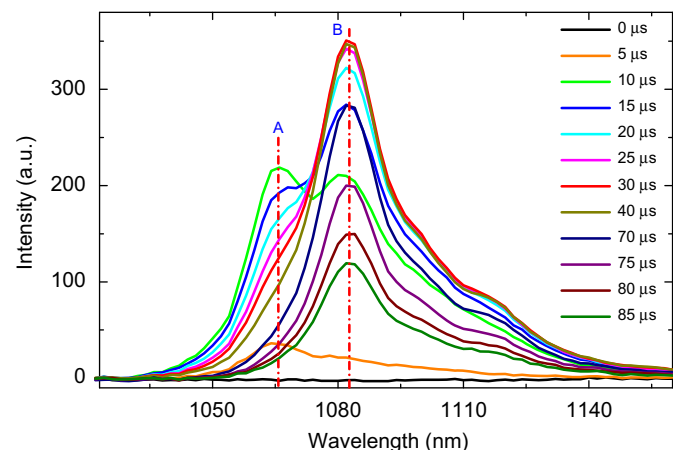


Fig. 3. The RT TRPL spectra of Nd^{3+} ions doped ZnO NCs obtained under the laser excitation at 811 nm.

Er^{3+} was characterized by a single exponential function when excited at 523.4 nm. The lifetimes of $^4S_{3/2}$ of Er^{3+} in TiO_2 NCs were determined to be 1.43 and 1.01 μs at 10 and 300 K, respectively. Moreover, it was found that the observed lifetime of $^4S_{3/2}$ of Er^{3+} remained nearly unaltered in the temperature range of 50–150 K (Fig. 4c). In sharp contrast, with increasing temperature from 150 to 300 K, $^4S_{3/2}$ lifetime decreased drastically.

Besides the single exponential decay behaviors, multi-exponential decays of Ln^{3+} could be also detected in Ln^{3+} ions doped semiconductor NCs. Fig. 5a illustrates the luminescence decay curves of MD transition of $^5D_0 \rightarrow ^7F_1$ of Eu^{3+} in $\text{SnO}_2:\text{Eu}^{3+}$ NCs at various temperatures when excited above the band-gap energy (~ 310 nm). It can be seen clearly that all the decay curves of Eu^{3+} exhibited obviously the multi-exponential nature, regardless of the low doping concentration (0.01 at%) of Eu^{3+} . Meanwhile, an unusually long decay of Eu^{3+} even up to several tens of seconds was observed in the tail owing to the trapping of carriers by some long-lived defect states in SnO_2 NCs. Further efforts on the investigation of the mechanism responsible for the long decay of Eu^{3+} are currently underway.

3.2. Dependence of PL lifetime on the non-solid medium around NCs

As discussed in Section 3.1, in nanoscale systems, there are many factors that may affect radiative and nonradiative decay rates and thus luminescence lifetimes of the dopants. The increase in surface-to-volume ratio in Ln^{3+} ions doped NCs will produce a

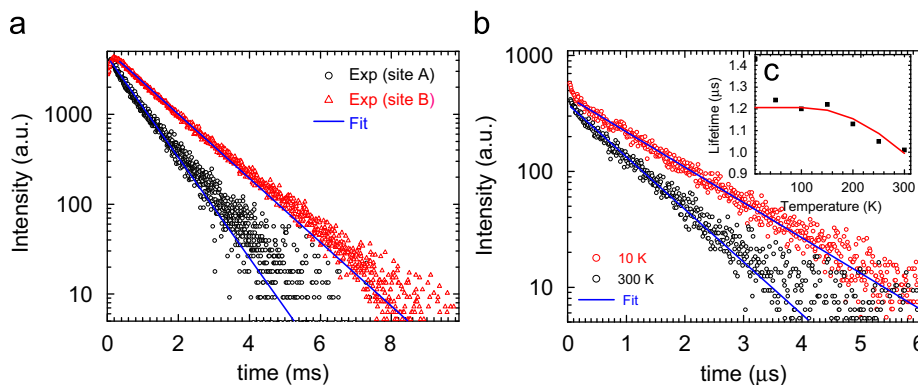


Fig. 4. (a) The 10 K luminescence decays from 5D_0 of Eu^{3+} at sites A and B in $\text{ZnO}:\text{Eu}^{3+}$ NCs under site-selective excitation at 464.8 and 467.8 nm, respectively; (b) luminescence decay of the $^4S_{3/2}$ state at 10 and 300 K under excitation at 523.4 nm and (c) temperature dependence of PL lifetime of $^4S_{3/2}$ in $\text{TiO}_2:\text{Er}^{3+}$ NCs, with the experimental (dotted) and fitted (solid) results.

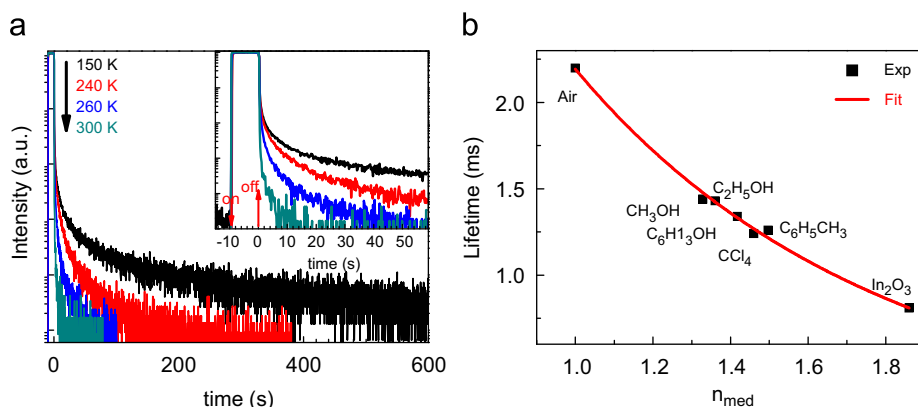


Fig. 5. (a) Long-lasting decay kinetics of Eu^{3+} in SnO_2 NCs at various temperatures recorded with FLS920 spectrometer. The luminescence system was brought to the steady state by continuous illuminating by a Xe lamp for 10 s, and the illumination was turned off at $t=0$, from then decay signals were recorded. All the decay curves were normalized to the luminescence intensity at $t=0$ and (b) dependence of 5D_0 lifetime of $\text{Eu}^{3+}(\text{C}_2)$ in In_2O_3 NCs on refractive index of the surrounding medium at RT.

large number of surface defect states or quenching centers, which may act as nonradiative relaxation channels (traps or killer sites). Consequently, PL lifetimes of Ln^{3+} ions in NCs are expected to decrease in comparison with their bulk counterparts [4]. On the contrary, luminescence lifetime of Ln^{3+} ions in some NCs has been reported to be longer relative to that in the bulk materials due to the effect of the non-solid medium surrounding NCs [25,26].

For Ln^{3+} ions embedding in semiconductor NCs, it was observed that lifetimes of Ln^{3+} ions depend strongly on the non-solid medium surrounding NCs. This phenomenon was mainly ascribed to the influence of effective refractive index of the surrounding medium on radiative lifetime, which could be well interpreted with the virtual-cavity model as $\tau_r \sim (1/f)(\lambda_0^2/\chi)$ [26,27], where $\chi = [1/2(n^2 + 2)]^2 n$ for the ED transition, $\chi = n^3$ for the MD transition, f is the oscillator strength for transitions in vacuum, λ_0 is the wavelength in vacuum and n the refractive index of the medium. For NCs with a size much smaller than the wavelength of light, n should be replaced by an effective index of refraction (n_{eff}). The effective index of refraction (n_{eff}) is defined as $n_{\text{eff}} = xn_{\text{np}} + (1-x)n_{\text{med}}$, where x is the filling factor showing what fraction of space is occupied by the NCs with a refractive index of n_{np} and n_{med} the refractive index of the medium. Taking the $\text{In}_2\text{O}_3:\text{Eu}^{3+}$ NCs for example, we have measured $^5\text{D}_0$ lifetimes of Eu^{3+} at C_2 site in In_2O_3 NCs immersed in solvents with different refractive indices [15]. The experimental data were used for fitting with the virtual-cavity model aforementioned. As shown in Fig. 5b, $^5\text{D}_0$ lifetime of Eu^{3+} was found to be significantly affected by the surrounding medium. Large refractive index of the surrounding medium resulted in small radiative lifetime of $^5\text{D}_0$

of Eu^{3+} . Similar fitting was also performed for the surface and lattice sites of Eu^{3+} in ZnO NCs using the virtual-cavity model [12].

4. Host sensitized luminescence

Although luminescence can be theoretically expected from all Ln^{3+} ions, efficient emissions of Ln^{3+} ions are usually generated via host sensitization in most cases. One of the advantages for Ln^{3+} doped semiconductor NCs is that the luminescence of Ln^{3+} ions can be efficiently sensitized by the exciton recombination in semiconductor NCs (Fig. 6), as previously established in Ln^{3+} ions doped TiO_2 , ZnO and SnO_2 NCs [10,12,13,17].

Fig. 7 shows the RT excitation and emission spectra of $\text{TiO}_2:\text{Nd}^{3+}$ and $\text{TiO}_2:\text{Sm}^{3+}$ NCs. Intense NIR PL of Nd^{3+} was observed on excitation above the TiO_2 band-gap at 345 nm. The emission lines centered at 915, 1094 and 1384 nm were due to the transitions from $^4\text{F}_{3/2}$ to $^4\text{I}_{9/2}$, $^4\text{I}_{11/2}$ and $^4\text{I}_{13/2}$, respectively (Fig. 7b), indicating that the Nd^{3+} emissions could be achieved via an efficient nonradiative ET process from TiO_2 to Nd^{3+} . This intriguing result was further evidenced by the presence of the intense band-gap absorption peak of anatase TiO_2 in the excitation spectrum of $\text{TiO}_2:\text{Nd}^{3+}$ NCs (Fig. 7a upper). Moreover, it should be noted that the excitation lines arising from 4f–4f transitions of Nd^{3+} itself in the RT excitation spectrum were hardly detectable, revealing the fact that the sensitized emission was a much more efficient pathway than the direct excitation of Nd^{3+} . The sensitized PL was also observed in $\text{TiO}_2:\text{Sm}^{3+}$ NCs in visible region. As shown in Fig. 7c, sharp emission lines of Sm^{3+} in the region 560–750 nm were detected on excitation above the TiO_2 band-gap at 343 nm at RT, producing an overall orange-to-red emission that was visible to the naked eye (Fig. 7d). The emission lines centered at 584.1, 612.8, 664.1 and 727.0 nm were readily assigned to the de-excitation from $^4\text{G}_{5/2}$ to its lower multiplets of $^6\text{H}_{5/2}$, $^6\text{H}_{7/2}$, $^6\text{H}_{9/2}$ and $^6\text{H}_{11/2}$, respectively. Similar to the case of $\text{TiO}_2:\text{Nd}^{3+}$ NCs, only much weaker excitation lines originating from Sm^{3+} itself were observed apart from the broad band-gap absorption peak of TiO_2 centered at 343 nm (Fig. 7a lower).

Fig. 8 exhibited the RT PL excitation and emission spectra of Er^{3+} and Eu^{3+} in SnO_2 NCs. Both the PL excitation spectra of Eu^{3+} and Er^{3+} were dominated by a strong UV broadband centered at ~ 310 nm, which corresponds to the band-gap absorption peak of SnO_2 NCs [13], whereas the emission spectra displayed the fingerprints of Eu^{3+} (Fig. 8b) and Er^{3+} (Fig. 8c) ions when indirectly excited at ~ 310 nm, suggesting that the Eu^{3+} and Er^{3+} emissions could be achieved via an ET process from the SnO_2 host

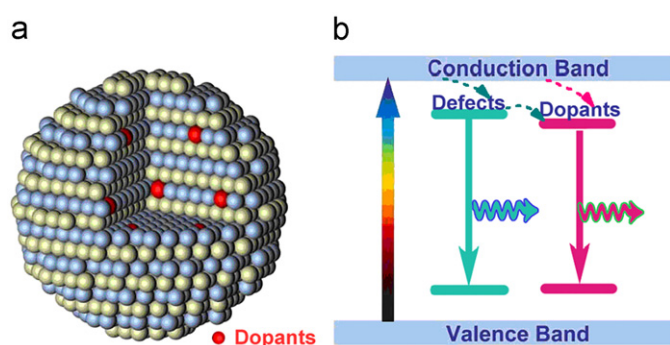


Fig. 6. Schematic illustration showing (a) the semiconductor NCs with Ln^{3+} ions embedded in the lattices and (b) ET processes responsible for the sensitized luminescence of the Ln^{3+} ions.

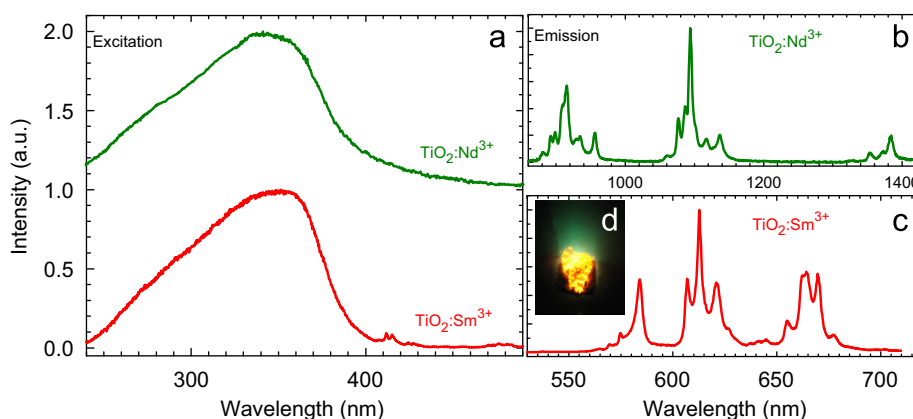


Fig. 7. Excitation (a) and emission (b, c) spectra for $\text{TiO}_2:\text{Nd}^{3+}$ and $\text{TiO}_2:\text{Sm}^{3+}$ NCs at RT and (d) exhibits PL photograph of $\text{TiO}_2:\text{Sm}^{3+}$ on excitation above the TiO_2 band-gap at 343 nm.

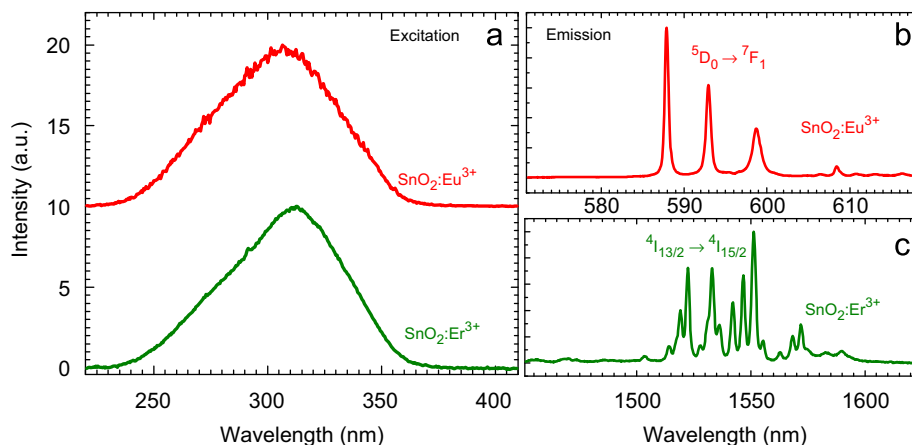


Fig. 8. Excitation (a) and emission (b, c) spectra for $\text{SnO}_2:\text{Eu}^{3+}$ and $\text{SnO}_2:\text{Er}^{3+}$ NCs at RT.

to emitters. In this process, the SnO_2 host served as a light-harvesting antenna (i.e. sensitizer) to absorb UV excitation light and subsequently transferred energy to the dopants, resulting in the intense MD luminescence of the $^5\text{D}_0 \rightarrow ^7\text{F}_1$ transition of Eu^{3+} and the $^4\text{I}_{13/2} \rightarrow ^4\text{I}_{15/2}$ transition of Er^{3+} .

Despite the fact that much significant progress has been made in Ln^{3+} ions doped semiconductor NCs, thorough and comprehensive understanding of the mechanism for ET from ZnO host to Ln^{3+} is still a great challenge. It has been reported that the various types of defect states in semiconductor NCs such as TiO_2 and ZnO played a crucial role in the ET between semiconductors and the doped Ln^{3+} ions [3,10,17]. However, solid evidence to reveal the mechanism of the ET process from the defect energy levels of the host to dopants has not yet been clarified so far. Time-resolved spectroscopy and single-particle (single-molecule) fluorescence spectroscopy may be very helpful to investigate the PL behaviors of Ln^{3+} ions in nanomaterials and the mechanism of host-to- Ln^{3+} ET.

5. Up-conversion luminescence

UC refers to nonlinear optical processes that convert two or more low-energy pump photons to a higher-energy output photon. In general, the practically useful UC luminescence occurs mainly via two basic mechanisms: ground state absorption/excited-state absorption (GSA/ESA) and energy transfer UC (ETU) [28,29]. Both the GSA/ESA and ETU processes take the form of consecutive absorption of two pump photons to populate the metastable levels and differ in that the ETU is realized through ET between two neighboring ions rather than successive absorption of two photons within single ion. The GSA/ESA and ETU processes can be readily distinguished from each other by virtue of the excitation spectra, luminescence decays and the concentration related optical properties of luminescent states of UC ions. For example, luminescence decay should present a single exponential nature if UC process is due to the GSA/ESA of single ion. In contrast, a rising edge in the initial stage may be observed in the luminescence decay curve for the ETU process, since the population of the luminescent level requires an ET between two ions.

As for Ln^{3+} ions in semiconductor NCs, such desired UC luminescence has been occasionally reported in TiO_2 and ZnO NCs [30]. In our recent work, intense UC emissions of Er^{3+} were achieved in $\text{TiO}_2:\text{Er}^{3+}$ and $\text{TiO}_2:\text{Yb}^{3+}, \text{Er}^{3+}$ NCs at RT (Fig. 9a). On excitation at 974.5 nm laser, the TiO_2 NCs singly doped with Er^{3+} exhibited sharp UC emission peaks in the regions 520–535,

535–575 and 650–690 nm, which were attributed to the $^2\text{H}_{11/2} \rightarrow ^4\text{I}_{15/2}$, $^4\text{S}_{3/2} \rightarrow ^4\text{I}_{15/2}$ and $^4\text{F}_{9/2} \rightarrow ^4\text{I}_{15/2}$ transitions of Er^{3+} , respectively (Fig. 9a lower). After co-doping 2.5 at% Yb^{3+} ions into $\text{TiO}_2:\text{Er}^{3+}$ NCs, a 5–6 fold enhancement in UC luminescence intensity of Er^{3+} was observed because of the much larger absorption cross-section of Yb^{3+} relative to that of Er^{3+} in the NIR region (Fig. 9a, upper).

To demonstrate the mechanism responsible for the UC emissions of Er^{3+} in TiO_2 NCs, the RT UC decays of $^4\text{S}_{3/2}$ of $\text{TiO}_2:\text{Er}^{3+}$ and $\text{TiO}_2:\text{Yb}^{3+}, \text{Er}^{3+}$ were recorded under the excitation of 974.5 nm. As shown in Fig. 9b, a rising edge at the initial stage of the decay curve was observed in $\text{TiO}_2:\text{Yb}^{3+}, \text{Er}^{3+}$ NCs, which was typical of the ET process from Yb^{3+} to Er^{3+} and thus established that the UC emissions of Er^{3+} were produced via an ETU process. By contrast, no such rise edge could be detected in Er^{3+} singly doped TiO_2 NCs, suggesting that the UC emissions of $\text{TiO}_2:\text{Er}^{3+}$ were achieved mainly through the GSA/ESA process. Meanwhile, the pump power dependence of the green and red UC emission intensities were also measured at RT. The resulting values of pump photon numbers (n) were determined to be 2.0 and 1.96 (Fig. 9c), respectively, indicative of the two-photon process involved in the population of the $^4\text{S}_{3/2}$ ($^2\text{H}_{11/2}$) and $^4\text{F}_{9/2}$ states of Er^{3+} in $\text{TiO}_2:\text{Er}^{3+}$ NCs. In the case of Yb^{3+} and Er^{3+} co-doped TiO_2 NCs, both the green and red UC emission intensities of Er^{3+} showed also quadratic power dependencies (Fig. 9d), indicative of the two-photon UC mechanism as previously established in $\text{ZnO}:\text{Er}^{3+}$ NCs [30].

6. Conclusions and outlook

Our recent work in Ln^{3+} ions doped wide band-gap semiconductor NCs was briefly reviewed with emphasis on PL properties, including electronic structures, luminescence dynamics, ET as well as UC emissions of Ln^{3+} ions in ZnO , TiO_2 , SnO_2 and In_2O_3 NCs, which were synthesized using wet chemical methods. Due to charge imbalance and/or large mismatch in ionic radius between Ln^{3+} and the host cations, multiple sites possessing various CF surroundings were formed after the introduction of Ln^{3+} ions into the lattices of wide band-gap semiconductor NCs. These distinct luminescence centers of Ln^{3+} ions could be unambiguously identified by means of site-selective and time-resolved spectroscopy at low temperature. Using Eu^{3+} as an optical probe, the local structure of Eu^{3+} in semiconductor NCs was revealed. In view of the diverse CF surroundings, such multiple sites of Ln^{3+} ions were usually characterized by very

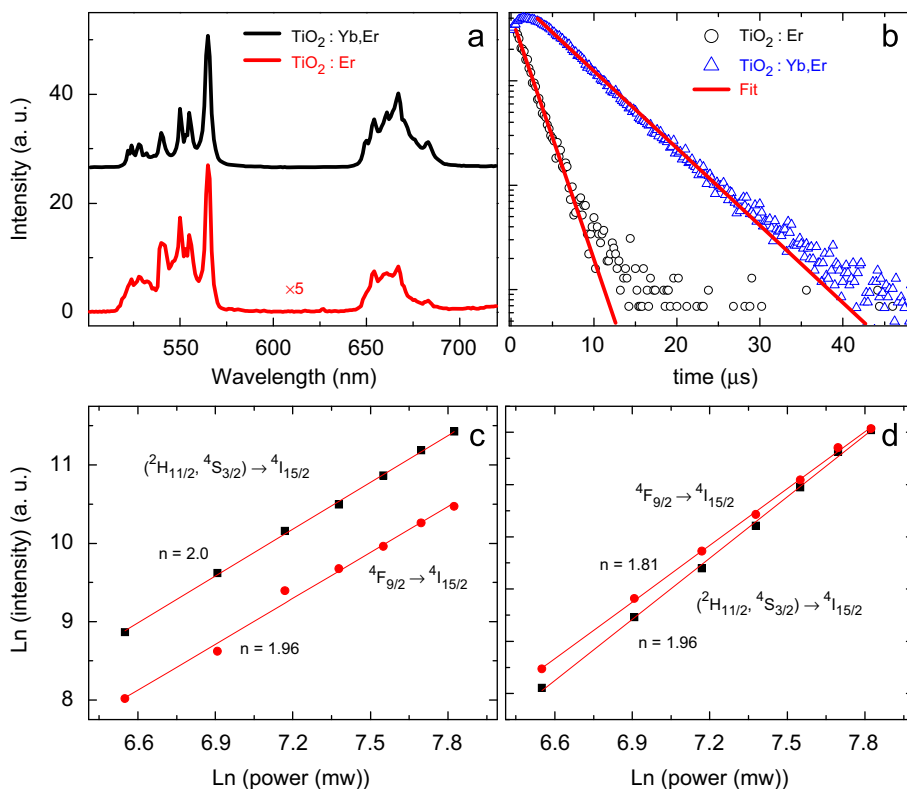


Fig. 9. (a) RT UC emission spectra for $\text{TiO}_2:\text{Er}^{3+}$ (lower) and $\text{TiO}_2:\text{Yb}^{3+}, \text{Er}^{3+}$ (upper) NCs; (b) UC luminescence decays of $\text{TiO}_2:\text{Er}^{3+}$ and $\text{TiO}_2:\text{Yb}^{3+}, \text{Er}^{3+}$ by monitoring the $^4\text{S}_{3/2} \rightarrow ^4\text{I}_{15/2}$ transition of Er^{3+} ions at RT; double logarithmic plots of the power dependence of integrated UC emission intensities of $^2\text{H}_{11/2}, ^4\text{S}_{3/2} \rightarrow ^4\text{I}_{15/2}$ and $^4\text{F}_{9/2} \rightarrow ^4\text{I}_{15/2}$ for (c) $\text{TiO}_2:\text{Er}^{3+}$ and (d) $\text{TiO}_2:\text{Yb}^{3+}, \text{Er}^{3+}$ NCs at RT under laser excitation at 974.5 nm.

different luminescence decays, which were found to be more complicated owing to the effect of NC surrounding medium and carrier traps. More importantly, it was observed that the host-to- Ln^{3+} ET was particularly efficient to sensitize specific Ln^{3+} ions such as Eu^{3+} , Er^{3+} in SnO_2 and Nd^{3+} , Sm^{3+} in TiO_2 NCs and then resulted in intense luminescence of Ln^{3+} ions from visible to NIR regions. It is believed that the sensitized luminescence of Ln^{3+} in semiconductor NCs will have many important applications in diverse fields such as optical devices and luminescent biolabels.

Although there are many reports describing the synthesis of Ln^{3+} doped wide band-gap semiconductor NCs, monodisperse and size-controllable semiconductor NCs with desirable properties and functions are still lacking so far. Considerable efforts are absolutely necessary to develop feasible synthetic strategy to fabricate monodisperse Ln^{3+} doped semiconductor NCs. Moreover, a more in-depth insight into the optical properties of such Ln^{3+} doped semiconductor NCs is still needed, which may be very important to optimize their optical performance for technological applications. Additional study methodologies such as extended X-ray-absorption fine structure (EXAFS), time-resolved spectroscopy and single-particle (single-molecule) luminescence spectroscopy will be helpful to the systematical investigation into the PL dynamics, the mechanism of host-to- Ln^{3+} energy transfer as well as the systematic CF analysis of local environment and distortion around Ln^{3+} ions.

Acknowledgments

This work is supported by the Hundred Talent Program of the Chinese Academy of Sciences (CAS), Knowledge Innovation

Program of CAS for Key Topics (No. KJXC2-YW-358), the NSFC (Nos. 10974200 and 10804106), the 973 and 863 programs of MOST (Nos. 2007CB936703 and 2009AA03Z430), NSF of Fujian Province for Distinguished Young Scholars (Nos. 2009J06030, 2009J05138 and 2010J05126).

References

- [1] F. Wang, Y. Han, C.S. Lim, Y.H. Lu, J. Wang, J. Xu, H.Y. Chen, C. Zhang, M.H. Hong, X.G. Liu, *Nature* 463 (2010) 1061.
- [2] Y.J. Sun, Y. Chen, L.J. Tian, Y. Yu, X.G. Kong, Q.H. Zeng, Y.L. Zhang, H. Zhang, *J. Lumin.* 128 (2008) 15.
- [3] T. Tachikawa, T. Ishigaki, J.-G. Li, M. Fujitsuka, T. Majima, *Angew. Chem. Int. Ed.* 47 (2008) 5348.
- [4] G.K. Liu, X.Y. Chen, in: K.A. Gschneidner Jr., J.C.G. Bunzli, V.K. Pecharsky (Eds.), *Handbook on the Physics and Chemistry of Rare Earths*, vol. 37, Elsevier Science B.V, Amsterdam 2007, p. 99.
- [5] J.B. Yin, L.Q. Xiang, X.P. Zhao, *Appl. Phys. Lett.* 90 (2007) 113112.
- [6] A.S. Pereira, M. Peres, M.J. Soares, E. Alves, A. Neves, T. Trindade, *Nanotechnology* 17 (2006) 834.
- [7] Y.P. Du, Y.W. Zhang, L.D. Sun, C.H. Yan, *J. Phys. Chem. C* 112 (2008) 12234.
- [8] L. Li, C.K. Tsung, Z. Yang, G.D. Stucky, L.D. Sun, J.F. Wang, C.H. Yan, *Adv. Mater.* 20 (2008) 903.
- [9] Y.S. Liu, W.Q. Luo, R.F. Li, H.M. Zhu, X.Y. Chen, *Opt. Express* 17 (2009) 9748.
- [10] W.Q. Luo, R.F. Li, X.Y. Chen, *J. Phys. Chem. C* 113 (2009) 8772.
- [11] W.Q. Luo, R.F. Li, G.K. Liu, M.R. Antonio, X.Y. Chen, *J. Phys. Chem. C* 112 (2008) 10370.
- [12] Y.S. Liu, W.Q. Luo, R.F. Li, G.K. Liu, M.R. Antonio, X.Y. Chen, *J. Phys. Chem. C* 112 (2008) 686.
- [13] J.T. Kong, H.M. Zhu, R.F. Li, W.Q. Luo, X.Y. Chen, *Opt. Lett.* 34 (2009) 1873.
- [14] C.Y. Fu, J.S. Liao, W.Q. Luo, R.F. Li, X.Y. Chen, *Opt. Lett.* 33 (2008) 953.
- [15] Q.B. Xiao, Y.S. Liu, L.Q. Liu, R.F. Li, W.Q. Luo, X.Y. Chen, *J. Phys. Chem. C* 114 (2010) 9314.
- [16] Y.S. Liu, W.Q. Luo, R.F. Li, X.Y. Chen, *Opt. Lett.* 32 (2007) 566.
- [17] X.Y. Zeng, J.L. Yuan, Z.Y. Wang, L. Zhang, *Adv. Mater.* 19 (2007) 4510.
- [18] P.A. Tanner, L.X. Yu, *J. Nanosci. Nanotechnol.* 8 (2008) 1307.
- [19] X.Y. Chen, G.K. Liu, *J. Solid State Chem.* 178 (2005) 419.

- [20] G.S. Ofelt, J. Chem. Phys. 37 (1962) 511.
- [21] B.R. Judd, Phys. Rev. 127 (1962) 750.
- [22] P.H. Butler, in: Point Group Symmetry Application: Method and Tables, Plenum, New York, 1981.
- [23] X.Y. Chen, W. Zhao, R.E. Cook, G.K. Liu, Phys. Rev. B 70 (2004) 205122.
- [24] M.F. Reid, f-shell empirical programs and examples, private communication.
- [25] L.Q. Liu, E. Ma, R.F. Li, G.K. Liu, X.Y. Chen, Nanotechnology 18 (2007) 015403.
- [26] R.S. Meltzer, S.P. Feofilov, B. Tissue, H.B. Yuan, Phys. Rev. B 60 (1999) R14012.
- [27] J.C. Boyer, F. Vetrone, J.A. Capobianco, A. Speghini, M. Bettinelli, J. Phys. Chem. B 108 (2004) 20137.
- [28] F. Wang, X.G. Liu, Chem. Soc. Rev. 38 (2009) 976.
- [29] F. Auzel, Chem. Rev. 104 (2004) 139.
- [30] X. Wang, X.G. Kong, G.Y. Shan, Y. Yu, Y.J. Sun, L.Y. Feng, K.F. Chao, S.Z. Lu, Y.J. Li, J. Phys. Chem. B 108 (2004) 18408.